Macromolecules

pubs.acs.org/Macromolecules Article

Poly(hydrazide−imide) Membranes with Enhanced Interchain Interaction for Highly Selective H_2/CO_2 Separation

Lele Guo, Yapeng Shi, Shanshan Wu, Jian Jin,* and Zhenggong Wang*

Cite This: *Macromolecules* 2023, 56, 3430−3439 Read Online

ACCESS | Metrics & More | Article Recommendations | Supporting Information

ABSTRACT: Membrane-based H_2/CO_2 separation plays a significant role in sustainable hydrogen production. However, due to the similar diffusion speed of H_2 and CO_2 in polymers, very few polymer membranes can effectively separate them, which largely limits the application of membrane technology in the hydrogen production process. In this work, a new polymer named poly(hydrazide−imide) (PHI) is synthesized by the polycondensation reaction of aromatic dianhydride with isophthalic dihydrazide and is used for H_2/CO_2 separation. Hydrazide, a typical polar molecule, is introduced into the polyimide backbone to induce the formation of a hydrogen bond network inside the polymer as confirmed by temperature-dependent infrared reflection spectroscopy. With further thermal annealing, intermolecular $\pi-\pi$ interaction is simultaneously strengthened as proved by fluorescence emission spectroscopy, UV−vis absorption spectroscopy, and wide-angle X-ray diffraction (WAXD) characterization. The synergistic effect of the H-bond and $\pi-\pi$ interaction efficiently enhances the interchain interaction and optimizes the polymer packing state. The obtained membranes demonstrate greatly improved H_2 permeabilities and H_2/CO_2 selectivity with the comprehensive separation performance surpassing the 2008 Robeson upper bound. The membranes also exhibit excellent CO_2 plasticization resistance up to 40 bar and stability in the long-time (>100 h) mixed gas separation test. The design of hydrazide-based polyimide polymer membrane provides a new route for preparing polymer materials for H_2/CO_2 separation.

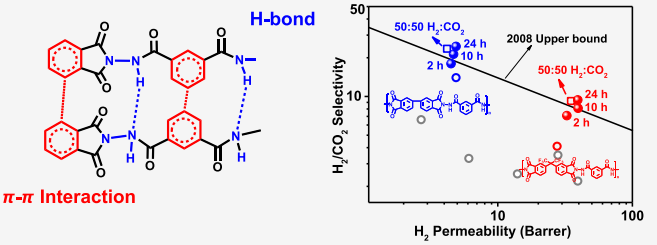

INTRODUCTION

Hydrogen energy has attracted widespread attention as a clean energy, especially with the breakthrough of fuel cell technology. At present, H_2 is mostly generated by steam reforming of fossil fuels followed by the water-gas shift reaction.[1] The produced H_2 is always mixed with CO_2 and must be purified before utilization. Membrane-based H_2 separation technology has be widely investigated due to its simplicity of operation and reduction in purification costs.[2,3] Inorganic membrane materials such as zeolites, MOFs, and 2D layered materials with confined pore size achieve superior H_2 and CO_2 separation performance due to the intense molecular sieve effect. However, there is an enormous challenge in the commercial-scale production of defect-free membranes with subnanometer channels.[4−10] Thus, commercial membranes currently used for gas separation are based on polymers owing to their good processability and ease of scale-up.[11] However, most conventional polymer membranes cannot distinguish H_2 and CO_2 molecules easily. Many attempts have been made to optimize the structure of polymer membranes for H_2 and CO_2 separation performance.[12−15]

The transportation of gas in polymeric membranes generally follows a solution-diffusion mechanism.[16] Gas permeability (P) is the product of its solubility (S) and diffusivity (D) in the polymer, and selectivity is determined by a combination of solubility selectivity and diffusivity selectivity. The solubility coefficient of polar molecule CO_2 is much larger than H_2 in the polymer, while the diffusion coefficient of H_2 is larger than CO_2 owing to the smaller size of H_2 molecule. One way to separate H_2 and CO_2 is to promote the preferential transfer of CO_2 by increasing the solubility selectivity of CO_2. However, the advantage of this membrane material lies in the removal of carbon dioxide, rather than obtaining high-purity hydrogen.[17] Another more recognized way is to use the small size difference between H_2 and CO_2 to promote the preferential permeation of H_2, that is, to improve the diffusion selectivity of H_2 to achieve H_2/CO_2 separation.[18] This separation mechanism is more conducive to obtain high-purity hydrogen. However, at present, polymer-based H_2/CO_2 separation membranes face a serious problem of low selectivity, and the H_2/CO_2 separation selectivity of most polymer membranes is lower than 3.[19−21] According to Freeman's theory, polymer interchain spacing and chain stiffness are the key parameters in determining their diffusion coefficients. To achieve high H_2/CO_2 selectivity,

Received: December 30, 2022
Revised: April 11, 2023
Published: April 25, 2023

https://doi.org/10.1021/acs.macromol.2c02594
Macromolecules 2023, 56, 3430−3439

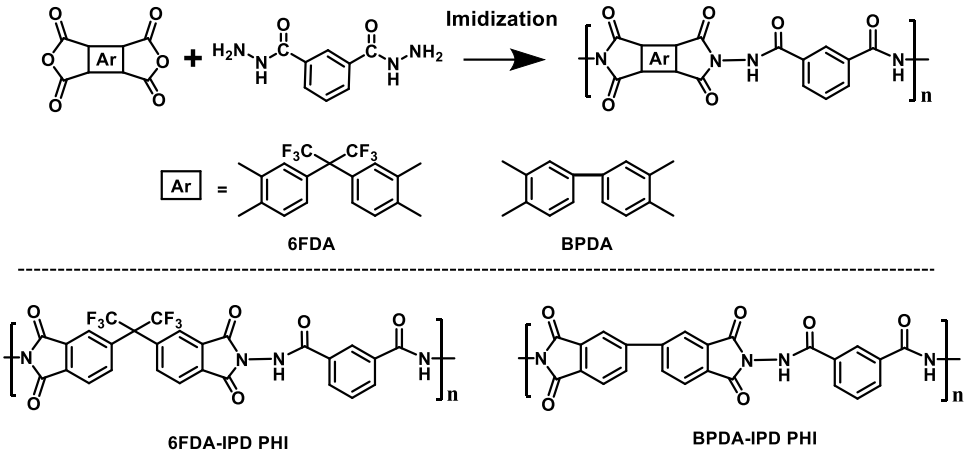

Figure 1. Synthesis route of two poly(hydrazide−imide)s.

polymers should have rigid chains with efficient chain packing to obtain high H_2/CO_2 diffusivity selectivity.[22] Among the present polymer materials, aromatic polymers interconnected with heterocyclic rings possess relatively high diffusion selectivity due to their rigid chain structure and dense chain packing. A heterocyclic polymer polybenzimidazole (PBI) emerged as one of the remarkable candidates for H_2/CO_2 separation with a selectivity of more than 6 at 35 °C. Because of its inherent interchain interaction, it shows high membrane density (1.27 g/mL) and denser chain packing than other glassy polymers.[23−25] To further increase chain rigidity and decrease free volumes, Lin's group reported the use of H_3PO_4 and terephthaloyl chloride to cross-link PBI to improve its size-sieving ability, thereby increasing the H_2/CO_2 selectivity by almost 100%.[12,26] In addition, H_2/CO_2 selectivity of polyimides could be improved via diamine cross-linking to manipulate chain rigidity and chain-packing efficiency. Chung's group reported that a polyimide (6FDA-durene) membrane could be cross-linked by various amines such as ethylenediamine (EDA), diethylenetriamine (DETA), diaminobutane (DAB) dendrimers, and other diamines, and H_2/CO_2 selectivity increased by more than 260%.[27−30] This approach involves the reaction of the imide ring of polyimide with a cross-linker molecule to produce a polymer network structure.[13,31−41] Their results showed that chemical cross-linking of polyimide membranes remains one of the most promising methods for improving H_2 enrichment. However, these methods mentioned above usually face several challenges: (1) only a few polymers with rigid structure that can be directly used to separate H_2 and CO_2; (2) the serious loss of permeability due to the denser chain packing after modification; (3) the destruction of the main chain of the polyimide caused by excessive reaction and the decrease of molecular weight of the polymer after cross-linking. Therefore, polymers with rationally designed structure for high-efficiency H_2/CO_2 separation is still highly desired.

The introduction of hydrogen-bond interaction is an important strategy to improve interchain interaction and adjust chain arrangement.[39,42] Poly(amide−imide)s (PAIs) always possess higher gas selectivity over polyimides owing to the additional hydrogen bonding within the polymers.[43,44] However, the H_2/CO_2 selectivity is still lower than required value. In this work, hydrazide is introduced into the polyimide backbone to induce a more abundant hydrogen-bond network inside the polymer membranes, aiming at enhancing H_2/CO_2 separation performance. Two hydrazide-based polyimides, 6FDA-IPD and BPDA-IPD, were synthesized by polycondensation reaction of 4,4′-(hexafluoroisopropylidene)diphthalic anhydride (6FDA) and 4,4′-biphthalic anhydride (BPDA) with isophthalic dihydrazide (IPD), respectively. Further thermal annealing of the polymer membranes induces simultaneously the generation intermolecular $\pi-\pi$ interaction. The synergistic effect of H-bond and $\pi-\pi$ interaction efficiently narrows the interchain *d*-spacing and sieving capacity for H_2 and CO_2. The H_2/CO_2 selectivity of the 6FDA-IPD membrane is up to 9.4, and that of the BPDA-IPD membrane is 24.5 with the comprehensive separation performance exceeding the 2008 Robeson upper bound. The membranes with enhanced interchain interaction also demonstrate superior CO_2 plasticization resistance up to 40 bar.

EXPERIMENTAL SECTION

Materials. 4,4′-(Hexafluoroisopropylidene)diphthalic anhydride (6FDA, 99.6%) and 4,4′-biphthalic anhydride (BPDA, 98%) were purchased from Tokyo Chemical Industrial Co. LTD and dried at 120 °C for 24 h under vacuum. Isophthalic dihydrazide (IPD, 95%) was purchased from Tokyo Chemical Industrial Co. Ltd. *N*-Methyl-2-pyrrolidone (NMP, 99.5%), dimethyl sulfoxide-d_6 (DMSO-d_6), and *N*,*N*-dimethylformamide (DMF, 99.5%) were purchased from Alfa Aesar. Methanol (99.5%) and toluene (99.5%) purchased from Sinopham Chemical Reagent Co. LTD were used as received.

Poly(hydrazide−imide) Membrane Preparation. *6FDA-IPD PHI membrane*: 20 mL of anhydrous NMP, IPD (1.94 g, 0.01 mol), and 6FDA (4.44 g, 0.01 mol) were added in a dried 100 mL flask under a nitrogen atmosphere. Anhydrous toluene (5 mL) was added into the mixture after 48 h stirring. Afterward, the temperature was gradually raised to 200 °C and held for 3 h. The resulting viscous solution was precipitated in methanol. The obtained sediment was collected by filtration, washed twice by methanol, and finally dried in a vacuum oven at 150 °C for 24 h. The resulting polymer was dissolved in DMF to form 5 wt % solution. The casting solution was poured into a 3 cm diameter circular glass mold supported by a leveled plate. The membranes were obtained by slow solvent evaporation for at least 36 h in dry oven under 60 °C and further heated at 150 °C for 24 h under high vacuum to remove any traces of residual DMF.

BPDA-IPD PHI membrane: The IPD (1.94 g, 0.01 mol) was dissolved in a flask with 15 mL of NMP. BPDA (2.94 g, 0.01 mol) was slowly added into the IPD solution followed by stirring for 48 h. The resulting poly(amino amic acid) (PAAc) solution was cast into a glass plate, stored overnight at 60 °C, then slowly heated to 200 °C, and thermal imidized in a vacuum oven. The preparation of BPDA-IPD

https://doi.org/10.1021/acs.macromol.2c02594
Macromolecules 2023, 56, 3430−3439

poly(hydrazide−imide) is different from that of 6FDA-IPD owing to the poor solubility of BPDA-IPD poly(hydrazide−imide) in NMP.

RESULTS AND DISCUSSION

Synthesis and Characterization of 6FDA-IPD and BPDA-IPD PHIs. Two poly(hydrazide−imide)s (PHIs) were prepared via a one-step solvothermal azeotropic cycloimidization reaction between the diamine monomer, isophthalic dihydrazide (IPD), and two dianhydride monomers, 4,4′-(hexafluoroisopropylidene)diphthalic anhydride (6FDA) and 4,4′-biphthalic anhydride (BPDA), as shown in Figure 1. The chemical structures of 6FDA-IPD and BPDA-IPD membranes are characterized by ATR-FTIR and ^{1}H NMR. As demonstrated in ATR-FTIR spectra in Figure 2a, the absorption

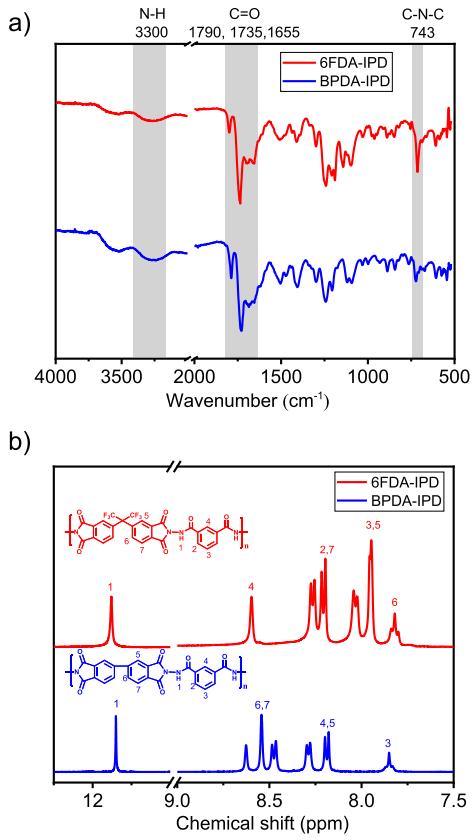

Figure 2. (a) ATR-FTIR spectra and (b) ^{1}H NMR spectra of two poly(hydrazide−imide) membranes.

bands of 1735, 1790, and 743 cm^{-1} are ascribed to the symmetric and asymmetric C═O and C−N−C stretch of imide groups. The adsorption band of 1655 cm^{-1} is ascribed to C═O in hydrazide groups, and the adsorption band of 3282 cm^{-1} belongs to the N−H stretching in hydrazide. The ^{1}H NMR spectrum is shown in Figure 2b. The signal at 11.7 ppm is attributed to the amino protons of hydrazide groups. The chemical shifts of 8.6−7.8 ppm are attributed to aromatic hydrogen atoms of poly(hydrazide−imide). These results determine the molecular structures precisely and indicate full imidization in the polymers. The membranes of 6FDA-IPD and BPDA-IPD poly(hydrazide−imide)s were fabricated via a solution-casting method. Stress−strain curves drawn in Figure S1 are measured to evaluate the mechanical properties of 6FDA-IPD and BPDA-IPD membranes. The tensile strength of 6FDA-IPD membrane is 106.9 MPa, the elongation is 6.6%, and Young's modulus is 2.6 GPa. The tensile strength of BPDA-IPD PHI membrane is 124.5 MPa, the elongation is 8.7%, and Young's modulus is 3.2 GPa. These results show that both poly(hydrazide−imide) membranes exhibit excellent mechanical properties.

Thermal Treatment of 6FDA-IPD and BPDA-IPD PHI Membranes. To strengthen interchain interaction, the 6FDA-IPD and BPDA-IPD PHI membranes were thermally annealed. The thermal treatment conditions are determined by TGA curves as shown in Figure 3. The two poly(hydrazide−imide)s

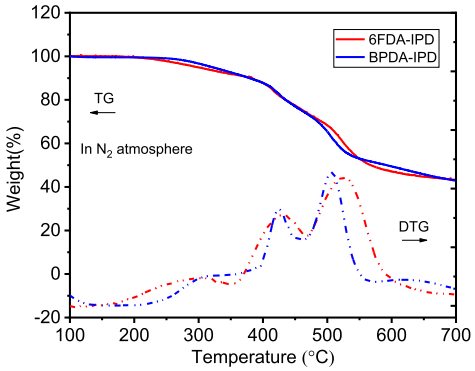

Figure 3. TGA (solid) and DTG (dotted) curves for 6FDA-IPD and BPDA-IPD PHI membranes.

undergo about 10% of weight loss at 400 °C, and the thermal stability is good enough for subsequent heat treatment. According to the analysis of TG curves, the 6FDA-IPD and BPDA-IPD PHI membranes were treated under 280 °C with different thermal treatment times (2, 10, and 24 h) using a tube furnace under a N_2 atmosphere.

The chemical structures of PHI membranes annealed for 24 h were characterized by ATR-FTIR as shown in Figure 4a. The absorption band at 743 cm^{-1} belonging to the imide group of both two annealed PHI membranes still exists, indicating the maintenance of main-chain structure under heating. In addition, N−H stretching in PHI membranes demonstrates an apparent red-shift after annealing from 3282 to 3288 cm^{-1}, indicating the slightly weakened hydrogen bond in annealed membranes. To further investigate hydrogen bond before and after annealing treatment in detail, temperature-dependent infrared reflection spectroscopy was performed (Figures 4b and 4c). The N−H stretching adsorption band moves to higher wavenumbers from 3282 and 3288 cm^{-1} to 3315 and 3319 cm^{-1} for 6FDA-IPD and 6FDA-IPD 280 °C−24 h PHI membranes, respectively. The results sufficiently verify the strong hydrogen-bond interaction in both two membranes. The 6FDA-IPD PHI membrane possesses the higher wavenumber shift of 33 cm^{-1} than 31 cm^{-1} of the 6FDA-IPD 280 °C−24 h membrane, reflecting a stronger hydrogen bond in the pristine 6FDA-IPD PHI membrane.

To characterize the variation of interchain interaction after annealing, 6FDA-IPD and BPDA-IPD PHI membranes were further characterized by fluorescence emission spectroscopy. As shown in Figures 5a and 5b, the fluorescence intensities of the 6FDA-IPD and BPDA-IPD PHI 280 °C−24 h membranes are lower than the pure 6FDA-IPD and BPDA-IPD PHI membranes. The attenuation in the fluorescence intensity of the annealed 6FDA-IPD and BPDA-IPD PHI membranes is attributed to the fluorescence quenching effect caused by enhanced $\pi-\pi$ interactions of the aromatic nucleus.[7,45,46] To

https://doi.org/10.1021/acs.macromol.2c02594
Macromolecules 2023, 56, 3430−3439

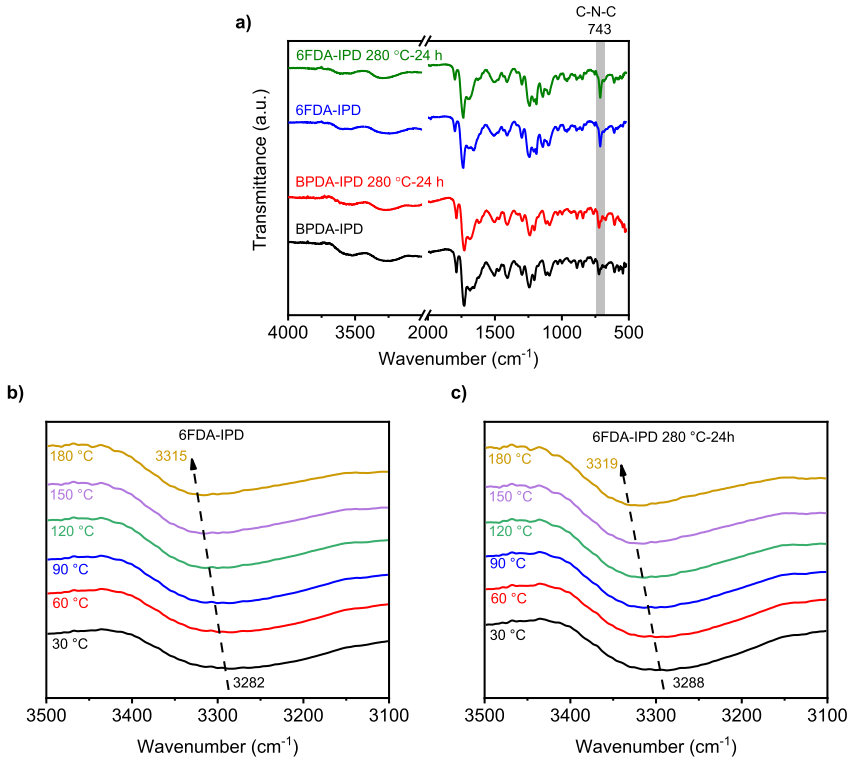

Figure 4. (a) ATR-FTIR spectra of 6FDA-IPD and BPDA-IPD membranes before and after thermal treatment. (b, c) Temperature-dependent infrared reflection spectra of 6FDA-IPD and 6FDA-IPD 280 °C−24 h membranes.

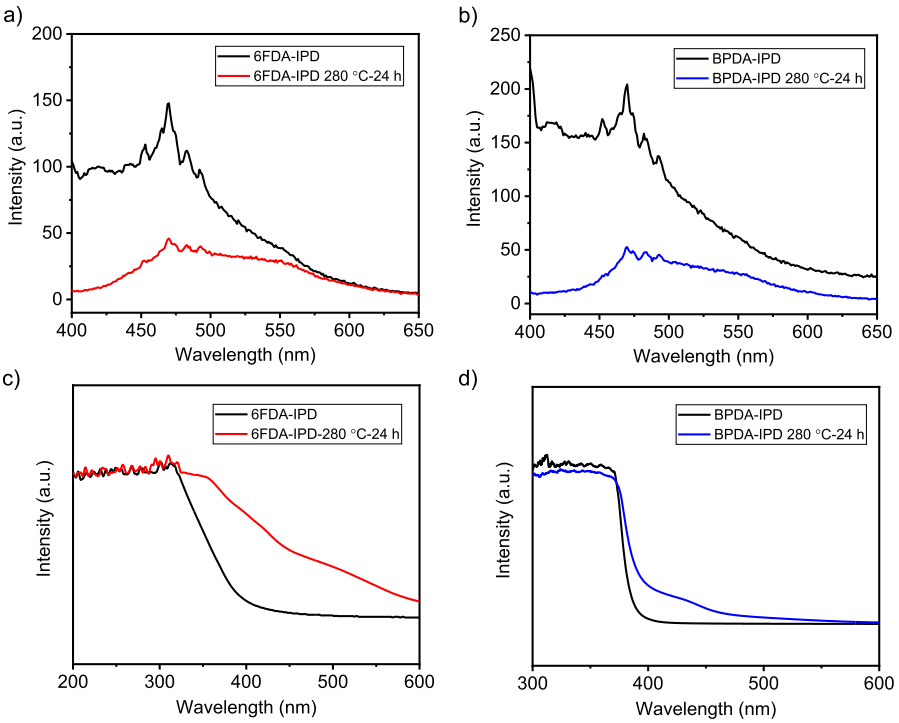

Figure 5. (a, b) Fluorescence emission spectra and (c, d) UV−vis absorption spectra of 6FDA-IPD and BPDA-IPD PHI membranes before and after thermal treatment.

further verify enhanced $\pi-\pi$ interactions, these membranes were characterized by UV−vis absorption spectroscopy. In the UV−vis absorption spectra of 6FDA-IPD and BPDA-IPD PHI membranes as shown in Figures 5c and 5d, the absorption peak at 312 and 369 nm are attributed to $\pi-\pi$ interactions between aromatic nucleus of 6FDA-IPD and BPDA-IPD PHI.[32,33] The absorption peaks move to 322 and 373 nm by annealing at 280 °C for 24 h. The red-shift proves a promoted $\pi-\pi$ transition between aromatic nucleus of 6FDA-IPD and BPDA-IPD PHI, which is probably attributed to the enhancement of the $\pi-\pi$

https://doi.org/10.1021/acs.macromol.2c02594
Macromolecules 2023, 56, 3430−3439

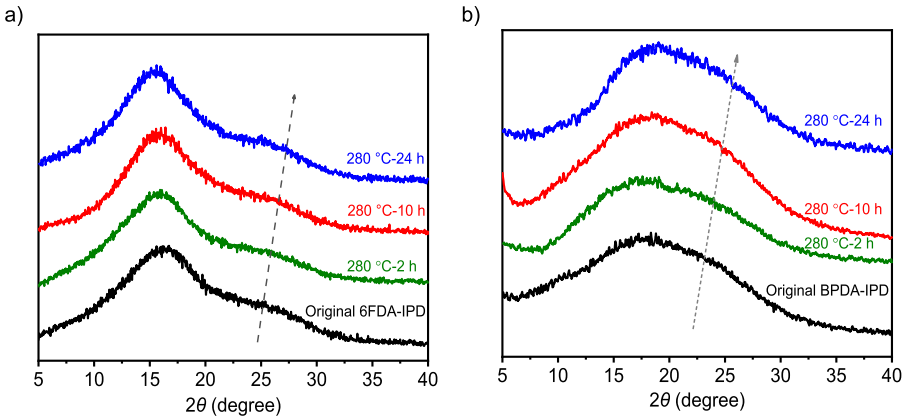

Figure 6. XRD patterns of (a) 6FDA-IPD and (b) BPDA-IPD PHI membranes before and after thermal treatment.

interaction. From the above analysis, we can infer that $\pi-\pi$ interactions are further enhanced after the annealing treatment.

To investigate the influence of thermal annealing on polymer chain packing state, the wide-angle X-ray diffraction (WAXD) of the membranes was characterized to estimate the variation of average interchain distance. As shown in Figure 6a,b, all the membranes have two broad diffraction peaks around 15° and 25°, which can be attributed to the typical interchain distance of polymer and the face-to-face $\pi-\pi$.[32] Figure 6a demonstrates the WAXD spectra of 6FDA-IPD membranes before and after thermal treatment. The peak related to $\pi-\pi$ stacking shifts from 25.4° to 27.2° with the increase of thermal annealing time, which indicates that the $\pi-\pi$ interactions are enhanced. However, the peak shifts gradually from 16.4°, corresponding to the *d* spacing of 5.39 Å, to 15.4°, corresponding to the *d* spacing of 5.75 Å, with the increase of thermal treatment time. The gradually increasing *d* spacing is possibly ascribed to the weakened hydrogen bonds during heating. In addition, the formation of $\pi-\pi$ interaction is partially hindered by the $-CF_3$ group with a large free volume, which also leads to the loose chain packing after heat treatment. In contrast, both two broad peaks of BPDA-IPD PHI membranes shift from 18.1° and 22.3° to 19.4° and 25.9° with increasing the thermal treatment time; correspondingly, the *d* spacing decreases from 4.89 to 4.56 Å as shown in Figure 6b. The result indicates that the $\pi-\pi$ interactions greatly strengthened after thermal treatment due to the existence of biphenyl structure in the BPDA-IPD, leading the *d* spacing to decrease. The density measurement and FFV calculation of the membrane[47,48] further confirm the effect of thermal annealing on the structure. The density of 6FDA-IPD decreases from 1.334 to 1.325 g/mL, and its FFV increases from 0.175 to 0.180 with the increase of annealing time at 280 °C as shown in Table S1. The density of BPDA-IPD increases from 1.457 to 1.461 g/mL, and its FFV decreases from 0.128 to 0.126 with the increase of annealing time at 280 °C. These results show that the chain spacing is regulated synergistically by interchain hydrogen bonds and $\pi-\pi$ interactions, which is schematically demonstrated in Figure 7.

The gas adsorption property of the 6FDA-IPD, 6FDA-IPD 280 °C−24 h, BPDA-IPD, and BPDA-IPD/280 °C−24 h PHI membranes were characterized by physisorption measurements. The CO_2 and H_2 adsorption isotherms at 273 K of membranes are shown in Figure 8. H_2 sorption is too low to measure accurately using our apparatus, indicating that there is almost no interaction force between polymers and H_2.[49−52]

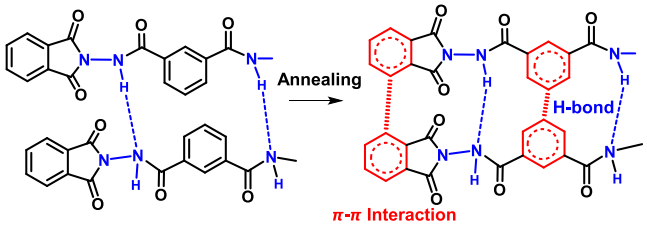

Figure 7. Interchain interaction of PHI membranes before and after thermal treatment.

The CO_2 adsorption capacities of pristine 6FDA-IPD and BPDA-IPD PHI membranes are 23.1 and 8.6 cm^3/g at 1.0 bar. With thermal treatment of 6FDA-IPD and BPDA-IPD PHI, the CO_2 adsorption capacity decreases to 18.1 and 3.4 cm^3/g. This is because the intermolecular $\pi-\pi$ packing effect is enhanced after thermal annealing, resulting in tighter chain spacing and reduced CO_2 adsorption.

Gas Separation Properties. The gas permeation properties of the membranes were measured on a fixed-volume pressure increase time-lag apparatus with feed gas at 4 bar and 35 °C. For each PHI membrane before and after thermal treatment, we tested no fewer than three samples and finally obtained the average value. The pure gas permeability and ideal selectivity are plotted in Figures 9a and 9b. The H_2 and CO_2 permeabilities of 6FDA-IPD PHI membrane are 27.6 and 6.7 barrer, respectively, and the ideal selectivity of H_2/CO_2 gas pair is 4.1. With the annealing time prolonging to 24 h, the H_2 permeability increased to 39.3 barrer and the H_2/CO_2 ideal selectivity increased to 9.4. As compared with pristine 6FDA-IPD PHI membrane, the increasing ratio of H_2 permeability and H_2/CO_2 ideal selectivity for 24 h annealed membrane are 42% and 129%, respectively. The increasing H_2 permeability with prolonging annealing time could be attributed to the enlarged *d* spacing or free volume obtained by WAXD spectra and FFV calculation, and the increased H_2/CO_2 ideal selectivity might be owing to the enhanced chain rigidity caused by the strengthened interchain interaction. As for the BPDA-IPD PHI membrane, the permeability of H_2 is 4.9 barrer and that of CO_2 is 0.35 barrer, which are much lower than that of the 6FDA-IPD PHI membrane. The H_2/CO_2 ideal selectivity of the BPDA-IPD PHI membrane is 14.0, which is much higher than that of the 6FDA-IPD PHI membrane, which could be attributed to the denser chain packing. With the increasing annealing time to 24 h, the ideal selectivity of H_2/CO_2 increased to 24.5 with 75% enhancement ratio of the

https://doi.org/10.1021/acs.macromol.2c02594
Macromolecules 2023, 56, 3430−3439

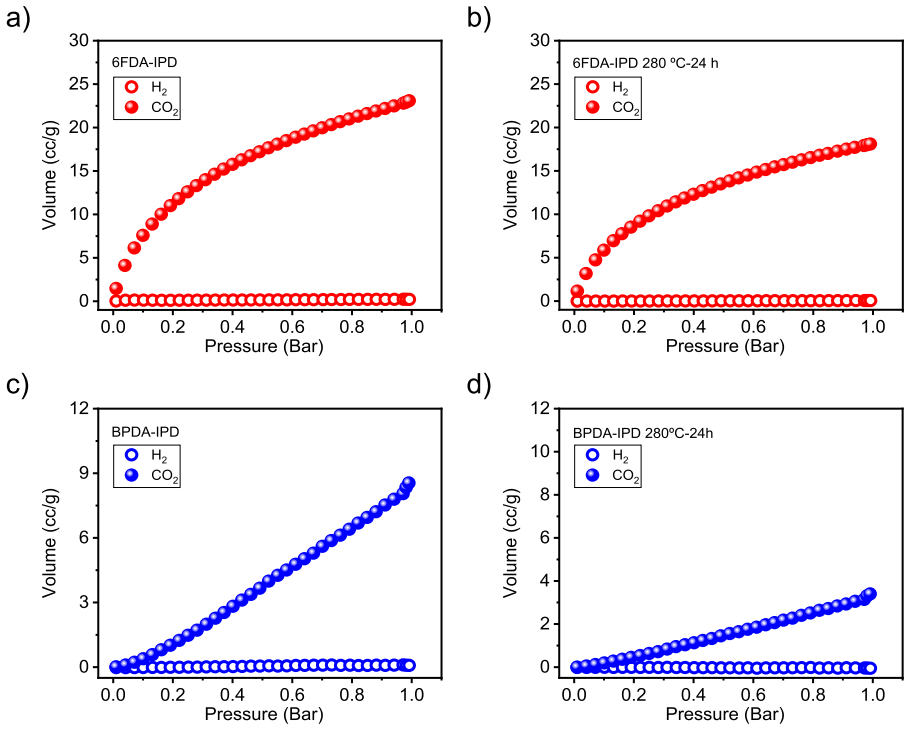

Figure 8. (a–d) H_2 and CO_2 sorption isotherms at 273 K for 6FDA-IPD and BPDA-IPD PHI membranes before and after thermal treatment.

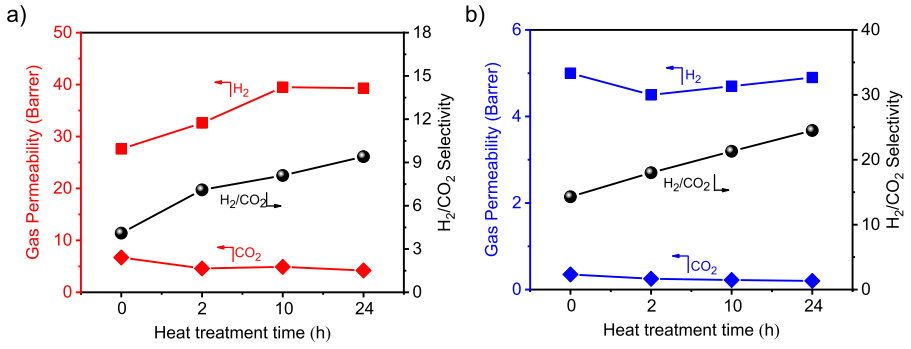

Figure 9. Influence on gas transport and gas pair separation properties of heat treatment time for 6FDA-IPD (a) and BPDA-IPD (b) PHI membranes.

pristine BPDA-IPD PHI membrane while the H_2 permeability almost unchanged. For both 6FDA-IPD and BPDA-IPD PHI membranes, the selectivity of H_2/CO_2 was largely improved by thermal annealing, reflecting the significant role of rationally enhancing interchain interaction on improving membrane separation capacity.

To further understand the gas transport mechanism of the PHIs membranes, the solubility coefficient (S), the diffusion coefficient (D), the solubility selectivity (α_D), and the diffusion (α_S) of the H_2/CO_2 gas pair are summarized. As shown in Table S3, the CO_2 solubility coefficients of 6FDA-IPD and BPDA-IPD are 3.03×10^{-1} and 1.13×10^{-1} cm^3 (STP)/cm^3·cmHg, which are much higher than 0.028×10^{-1} and 0.011×10^{-1} cm^3 (STP)/cm^3·cmHg for their H_2 solubility coefficients. Both H_2 and CO_2 solubility coefficients of 6FDA-IPD are larger than those of BPDA-IPD. The H_2 diffusion coefficients of 6FDA-IPD and BPDA-IPD are 985.7×10^{-9} and 445×10^{-9} cm^2/s, which are much higher than 2.2×10^{-9} and 0.3×10^{-9} cm^2/s for their CO_2 solubility coefficients. Both H_2 and CO_2 diffusion coefficients of 6FDA-IPD are larger than those of BPDA-IPD. With annealing treatment, H_2 diffusion coefficients of 6FDA-IPD PHI membrane improve from 985.7×10^{-9} to 4851.9×10^{-9} cm^2/s, and the CO_2 diffusion coefficient slightly decrease from 2.2×10^{-9} to 1.7×10^{-9} cm^2/s. The resulting H_2/CO_2 diffusion selectivity of 6FDA-IPD and BPDA-IPD PHIs membranes is 448.0 and 1483.3. The H_2/CO_2 solubility selectivity of the 6FDA-IPD and BPDA-IPD PHIs membranes is 0.0092 and 0.0098, which are basically the same as other polymers such as Matrimid 5218.[53] With annealing treatment, the H_2/CO_2 diffusion selectivity of 6FDA-IPD PHI membrane largely increases from 448.0 to 2854.1, while its solubility selectivity decreases from 0.0092 to 0.0034, reflecting the apparently enhanced diffusion-controlled separation mechanism.

The Robeson upper bound of the poly(hydrazide–imide) and thermally treated membranes for the gas pair of H_2/CO_2 is plotted in Figure 10a. They show that the gas separation performance for H_2/CO_2 of membranes that were thermally treated over 10 h exceeds the 2008 upper bound.[54] Moreover, the annealed PHI membranes located at much higher positions

https://doi.org/10.1021/acs.macromol.2c02594
Macromolecules 2023, 56, 3430–3439

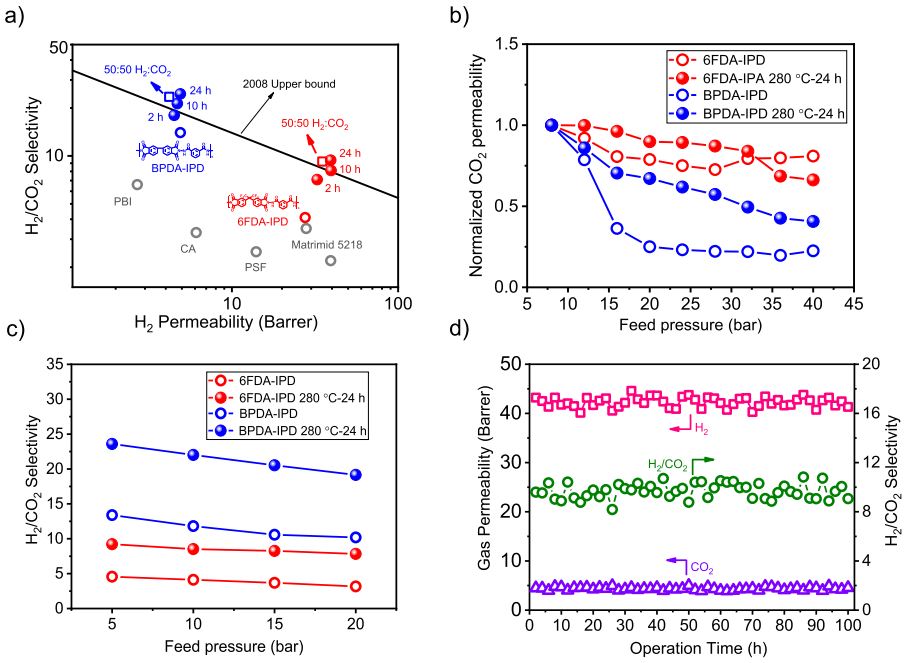

Figure 10. (a) Relationship between gas permeability and selectivity with 2008 upper bound for H_2/CO_2 gas pair. (b) Variation of CO_2 permeability with increased feed-gas pressure and (c) variation of selectivity of H_2/CO_2 in mixed H_2 and CO_2 for the 6FDA-IPD and BPDA-IPD PHI membranes before and after thermal treatment. (d) Long-term separation performance of 6FDA-IPD 280 °C−24 h membrane with 5 bar feed gas and at 35 °C.

in the upper bound plots as compared to some traditional polymers, such as PBI, CA, and PSF.[31,55,56] The excellent H_2/CO_2 separation performance of the annealed PHI membranes proves the significance of the synergistically enhanced hydrogen-bond and $\pi-\pi$ interactions.

Plasticization usually brings a serious loss in membrane selectivity as a result of polymer chain swelling on exposure to high pressure of polar gases. In general, the gas permeability of a glassy polymer membrane will decrease first and then increase with increasing pressure of the feed gas. The pressure corresponding to the minimum point is known as the plasticization pressure. Figure 10b represents the normalized CO_2 permeability isotherm for all 6FDA-IPD and BPDA-IPD PHI membranes with feed gas pressure ranging from 6 to 40 bar. The original 6FDA-IPD PHI membrane undergoes plasticization at the CO_2 partial pressure of 28 bar while the BPDA-IPD PHI membrane was not plasticized when the pressure was increased to 40 bar. Similarly, the plasticization did not occur in thermally treated membranes, revealing an excellent antiplasticization property of the resulting membranes. To judge the real appropriateness of the membranes, the gas separation performance of the pristine PHI and annealed PHI membranes was further evaluated using the 50:50 (vol/%) H_2/CO_2 mixed gas feed stream at elevated pressure. As shown in Figure 10c, a decrease in selectivity by increasing pressure was observed. As for the 6FDA-IPD PHI membrane, the increased feed gas pressure from 5 to 20 bar leads to the 36.3% decrease of H_2/CO_2 selectivity, and the selectivity of 6FDA-IPD 280 °C−24 h PHI membrane decreases by 23.3%. Meanwhile, the H_2/CO_2 selectivity of the BPDA-IPD PHI membrane decreases from 13.1 to 9.4, which decreases by 28.2%, while that of BPDA-IPD 280 °C-24 h PHI membrane decreases by 21.3%. The results of mixed gas permeation experiments further prove that the membranes after thermally treating have better plasticization resistance.

Extensive investigations have demonstrated that glassy polymer membranes tend to lose their permeability under long-term operation due to the reduction of fractional free volume. The long-term stability of 6FDA-IPD 280 °C−24 h PHI membrane was monitored by measuring the separation performance of mixed gas of H_2 and CO_2 (50:50 vol %) over time at 35 °C and 5 bar. As shown in Figure 10d, the CO_2 permeability and H_2/CO_2 selectivity remain almost unchanged during the test time, indicating the long-term stability of 6FDA-IPD 280 °C−24 h PHI membrane.

CONCLUSIONS

In this work, two novel poly(hydrazide−imide)s are first synthesized and then thermally annealed to achieve highly selective H_2/CO_2 separation. The incorporation of a polar molecule, hydrazide, induces the formation of a hydrogen-bond network inside the polymer, which is confirmed by temperature-dependent infrared reflection spectra. After thermal annealing, $\pi-\pi$ interaction is further strengthened in the membranes as verified by fluorescence emission spectra and UV−vis spectra. With thermal annealing, the hydrogen-bond interaction is weakened, and the $\pi-\pi$ interaction is enhanced inside the polymer chain. The synergistic effect of the hydrogen-bond network and the $\pi-\pi$ interaction rationally tunes interchain cavity and improves the molecular sieving property of the resulting membrane. The thermally annealed poly(hydrazide−imide) membranes exhibit superior H_2/CO_2 separation performance over present polymer membranes including PBI, CA, and PSF, surpassing the 2008 Robeson upper bound. In addition, theses membranes exhibit excellent long-term stability and improved plasticization resistance. Our work has demonstrated the possibility of poly(hydrazide−imide)s in the field of hydrogen separation and opens a new door for the design of polymer membranes for H_2/CO_2 separation.

https://doi.org/10.1021/acs.macromol.2c02594
Macromolecules 2023, 56, 3430−3439

■ ASSOCIATED CONTENT

Supporting Information

The Supporting Information is available free of charge at https://pubs.acs.org/doi/10.1021/acs.macromol.2c02594.

Stress−strain curves; density data, FFV data and *d*-spacing data of PHIs before and after annealing; diffusion coefficient data and solubility coefficient data of H_2 and CO_2 of PHIs before and after annealing; diffusion selectivity data and solubility selectivity data of H_2/CO_2 of PHIs before and after annealing; mixed-gas H_2 and CO_2 permeability and H_2/CO_2 selectivity data tested at 3 bar with 35 and 80 °C (PDF)

■ AUTHOR INFORMATION

Corresponding Authors

Zhenggong Wang − *College of Chemistry, Chemical Engineering and Materials Science & Collaborative Innovation Center of Suzhou Nano Science and Technology & Innovation Center for Chemical Science, Soochow University, Suzhou 215123, P. R. China; Jiangsu Key Laboratory of Advanced Negative Carbon Technologies, Soochow University, Suzhou 215123 Jiangsu, P. R. China*; Email: zgwang2017@suda.edu.cn

Jian Jin − *College of Chemistry, Chemical Engineering and Materials Science & Collaborative Innovation Center of Suzhou Nano Science and Technology & Innovation Center for Chemical Science, Soochow University, Suzhou 215123, P. R. China; Jiangsu Key Laboratory of Advanced Negative Carbon Technologies, Soochow University, Suzhou 215123 Jiangsu, P. R. China*; orcid.org/0000-0003-0429-300X; Email: jjin@suda.edu.cn

Authors

Lele Guo − *College of Chemistry, Chemical Engineering and Materials Science & Collaborative Innovation Center of Suzhou Nano Science and Technology & Innovation Center for Chemical Science, Soochow University, Suzhou 215123, P. R. China*

Yapeng Shi − *College of Chemistry, Chemical Engineering and Materials Science & Collaborative Innovation Center of Suzhou Nano Science and Technology & Innovation Center for Chemical Science, Soochow University, Suzhou 215123, P. R. China*

Shanshan Wu − *College of Chemistry, Chemical Engineering and Materials Science & Collaborative Innovation Center of Suzhou Nano Science and Technology & Innovation Center for Chemical Science, Soochow University, Suzhou 215123, P. R. China*

Complete contact information is available at: https://pubs.acs.org/10.1021/acs.macromol.2c02594

Author Contributions

L.G. and Y.S. contributed equally to this work. Z.W. and J.J.: initial idea and experimental design; L.G., Y.S., and S.W.: experiment and characterization; all authors: analysis and comments; Z.W. and J.J.: supervision: L.G. and Z.W.: writing-original draft; L.G., Z.W., and J.J.: writing-review and editing.

Notes

The authors declare no competing financial interest.

■ ACKNOWLEDGMENTS

This work was supported by the National Natural Science Foundation of China (21988102, 51873230) and the Key Development Project of Jiangsu Province (BE2022056). We thank the support from Jiangsu Key Laboratory of Advanced Functional Polymer Design and Application, Soochow University.

■ REFERENCES

(1) Ockwig, N. W.; Nenoff, T. M. Membranes for hydrogen separation. *Chem. Rev.* **2007**, *107*, 4078−4110.

(2) Peng, Y.; Li, Y. S.; Ban, Y. J.; Jin, H.; Jiao, W. M.; Liu, X. L.; Yang, W. S. Metal-organic framework nanosheets as building blocks for molecular sieving membranes. *Science* **2014**, *346*, 1356−1359.

(3) Stern, S. A. Polymers for gas separations: the next decade. *J. Membr. Sci.* **1994**, *94*, 1−65.

(4) Wang, Z. G.; Tian, Y. Y.; Fang, W. X.; Shrestha, B. B.; Huang, M. H.; Jin, J. Constructing strong interfacial interactions under mild conditions in MOF-incorporated mixed matrix membranes for gas separation. *ACS Appl. Mater. Interfaces.* **2021**, *13*, 3166−3174.

(5) Bi, X. Y.; Zhang, Y. A.; Zhang, F.; Zhang, S. X.; Wang, Z. G.; Jin, J. MOF nanosheet-based mixed matrix membranes with metal-organic coordination interfacial Interaction for gas separation. *ACS Appl. Mater. Interfaces.* **2020**, *12*, 49101−49110.

(6) Huang, A. S.; Caro, J. Covalent post-functionalization of zeolitic imidazolate framework ZIF-90 membrane for enhanced hydrogen selectivity. *Angew. Chem., Int. Ed.* **2011**, *50*, 4979−4982.

(7) Karthik, P.; Vinoth, R.; Zhang, P.; Choi, W.; Balaraman, E.; Neppolian, B. $\pi-\pi$ interaction between metal-organic framework and reduced graphene oxide for visible-light photocatalytic H_2 production. *ACS Appl. Energy Mater.* **2018**, *1*, 1913−1923.

(8) Rodenas, T.; Luz, I.; Prieto, G.; Seoane, B.; Miro, H.; Corma, A.; Kapteijn, F.; Llabres i Xamena, F. X.; Gascon, J. Metal-organic framework nanosheets in polymer composite materials for gas separation. *Nat. Mater.* **2015**, *14*, 48−55.

(9) Li, Y. J.; Liu, H. O.; Wang, H. T.; Qiu, J. S.; Zhang, X. F. GO-guided direct growth of highly oriented metal-organic framework nanosheet membranes for H_2/CO_2 separation. *Chem. Sci.* **2018**, *9*, 4132−4141.

(10) Yang, F. F.; Wu, M.; Wang, Y. C.; Ashtiani, S.; Jiang, H. Q. A GO-Induced assembly strategy to repair MOF nanosheet-based membrane for efficient H_2/CO_2 Separation. *ACS Appl. Mater. Interfaces.* **2019**, *11*, 990−997.

(11) Wang, Z. G.; Ren, H. T.; Zhang, S. X.; Zhang, F.; Jin, J. Polymers of intrinsic microporosity/metal-organic framework hybrid membranes with improved interfacial interaction for high-performance CO_2 separation. *J. Mater. Chem. A* **2017**, *5*, 10968−10977.

(12) Zhu, L. X.; Swihart, M. T.; Lin, H. Q. Tightening polybenzimidazole (PBI) nanostructure via chemical cross-Linking for membrane H_2/CO_2 separation. *J. Mater. Chem. A* **2017**, *5*, 19914−19923.

(13) Zhang, G.; Li, B.; Zhou, Y.; Chen, X.; Li, B.; Lu, Z.-Y.; Wu, L. Processing supramolecular framework for free interconvertible liquid separation. *Nat. Commun.* **2020**, *11*, 425.

(14) Yavari, M.; Fang, M.; Nguyen, H.; Merkel, T. C.; Lin, H.; Okamoto, Y. Dioxolane-based perfluoropolymers with superior membrane gas separation properties. *Macromolecules* **2018**, *51*, 2489−2497.

(15) Wang, Z. G.; Wang, D.; Zhang, F.; Jin, J. Tröger's base-based microporous polyimide membranes for high-performance gas separation. *ACS Macro Lett.* **2014**, *3*, 597−601.

(16) Kumar, A.; Huang, L.; Hu, L. Q.; Yin, D. Q.; Lin, H. Q.; Swihart, M. T. Facile one-pot synthesis of Pdm (M = Ag, Ni, Cu, Y) nanowires for use in mixed matrix membranes for efficient hydrogen separation. *J. Mater. Chem. A* **2021**, *9*, 12755−12762.

(17) Zhu, L. X.; Yin, D. Q.; Qin, Y. L.; Konda, S.; Zhang, S.; Zhu, A. D.; Liu, S.; Xu, T.; Swihart, M. T.; Lin, H. Q. Sorption-enhanced mixed matrix membranes with facilitated hydrogen transport for

hydrogen purification and CO_2 Capture. *Adv. Funct. Mater.* **2019**, *29*, 1904357.
(18) Pérez-Francisco, J. M.; Santiago-García, J. L.; Loría-Bastarrachea, M. I.; Paul, D. R.; Freeman, B. D.; Aguilar-Vega, M. Aguilar-Vega, CMS membranes from PBI/PI blends: Temperature effect on gas transport and separation performance. *J. Membr. Sci.* **2020**, *597*, No. 117703.
(19) Du, N. Y.; Dal-Cin, M.; Robertson, G. P.; Guiver, M. D. Decarboxylation-induced cross-Linking of polymers of intrinsic microporosity (PIMs) for membrane gas separation. *Macromolecules* **2012**, *45*, 5134−5139.
(20) Wang, Z. G.; Ren, H. T.; Zhang, S. X.; Zhang, F.; Jin, J. Carbon molecular sieve membranes derived from Troger's base-based microporous polyimide for gas separation. *ChemSusChem* **2018**, *11*, 916−923.
(21) Wu, J.; Liang, C. Z.; Naderi, A.; Chung, T. S. Tunable supramolecular cavities molecularly homogenized in polymer membranes for ultraefficient precombustion CO_2 capture. *Adv. Mater.* **2022**, *34*, 2105156.
(22) Ding, L.; Wei, Y. Y.; Li, L. B.; Zhang, T.; Wang, H. H.; Xue, J.; Ding, L. X.; Wang, S. Q.; Caro, J.; Gogotsi, Y. MXene molecular sieving membranes for highly efficient gas separation. *Nat. Commun.* **2018**, *9*, 155.
(23) Hu, L. Q.; Bui, V. T.; Krishnamurthy, A.; Fan, S. H.; Guo, W. J.; Pal, S.; Chen, X. Y.; Zhang, G. Y.; Ding, Y. F.; Singh, R. P.; Lupion, M.; Lin, H. Q. Tailoring sub-3.3 Å ultramicropores in advanced carbon molecular sieve membranes for blue hydrogen production. *Sci. Adv.* **2022**, *8*, No. eabl8160.
(24) Hu, L. Q.; Bui, V. T.; Huang, L.; Singh, R. P.; Lin, H. Q. Facilely cross-linking polybenzimidazole with polycarboxylic acids to improve H_2/CO_2 separation performance. *ACS Appl. Mater. Interfaces.* **2021**, *13*, 12521−12530.
(25) Hu, L. Q.; Fan, S. H.; Huang, L.; Bui, V. T.; Tran, T.; Chen, K. W.; Ding, Y. F.; Swihart, M. T.; Lin, H. Q. Supramolecular polymer networks of ion-coordinated polybenzimidazole with simultaneously improved H_2 permeability and H_2/CO_2 selectivity. *Macromolecules* **2022**, *55*, 6901−6910.
(26) Zhu, L. X.; Swihart, M. T.; Lin, H. Q. Unprecedented size-sieving ability in polybenzimidazole doped with polyprotic acids for membrane H_2/CO_2 separation. *Energy. Environ. Sci.* **2018**, *11*, 94−100.
(27) Low, B. T.; Xiao, Y. C.; Chung, T. S.; Liu, Y. Simultaneous occurrence of chemical grafting, cross-linking, and etching on the surface of polyimide membranes and their impact on H_2/CO_2 separation. *Macromolecules* **2008**, *41*, 1297−1309.
(28) Chung, T. S.; Shao, L.; Tin, P. S. Surface modification of polyimide membranes by diamines for H_2 and CO_2 separation. *Macromol. Rapid Commun.* **2006**, *27*, 998−1003.
(29) Shao, L.; Lau, C. H.; Chung, T. S. A novel strategy for surface modification of polyimide membranes by vapor-phase ethylenediamine (EDA) for hydrogen purification. *Int. J. Hydrogen. Energy* **2009**, *34*, 8716−8722.
(30) Wang, H.; Paul, D. R.; Chung, T. S. Surface modification of polyimide membranes by diethylenetriamine (DETA) vapor for H_2 purification and moisture effect on gas permeation. *J. Membr. Sci.* **2013**, *430*, 223−233.
(31) Yong, W. F.; Li, F. Y.; Chung, T. S.; Tong, Y. W. Highly permeable chemically modified PIM-1/Matrimid membranes for green hydrogen purification. *J. Mater. Chem. A* **2013**, *1*, 13914−13925.
(32) Kawakami, H.; Mikawa, M.; Nagaoka, S. Gas transport properties in thermally cured aromatic polyimide membranes. *J. Membr. Sci.* **1996**, *118*, 223−230.
(33) Shi, Y. S.; Wang, Z. G.; Shi, Y. P.; Zhu, S. W.; Zhang, Y. T.; Jin, J. Synergistic design of enhanced $\pi-\pi$ interaction and decarboxylation cross-linking of polyimide membranes for natural gas separation. *Macromolecules* **2022**, *55*, 2970−2982.
(34) Feng, Y.; Chen, S.; Jiang, D.; Li, H.; Hua, K.; Zhao, D.; Deng, M.; Ren, J. Thermal-oxidative membranes based on block hydroxyl polyimide for H_2 separation. *Macromolecules* **2022**, *55*, 370−381.
(35) He, S.; Jiang, X.; Li, S.; Ran, F.; Long, J.; Shao, L. Intermediate thermal manipulation of polymers of intrinsic microporous (PIMs) membranes for gas separations. *AIChE J.* **2020**, *66*, No. e16543.
(36) Wang, Z. G.; Wang, D.; Jin, J. Microporous polyimides with rationally designed chain structure achieving high performance for gas separation. *Macromolecules* **2014**, *47*, 7477−7483.
(37) Zhuang, Y. B.; Seong, J. G.; Do, Y. S.; Jo, H. J.; Cui, Z. L.; Lee, J.; Lee, Y. M.; Guiver, M. D. Intrinsically microporous soluble polyimides incorporating Tröger's base for membrane gas separation. *Macromolecules* **2014**, *47*, 3254−3262.
(38) Ying, Y.; Tong, M.; Ning, S.; Ravi, S. K.; Peh, S. B.; Tan, S. C.; Pennycook, S. J.; Zhao, D. Ultrathin two-dimensional membranes assembled by ionic covalent organic nanosheets with reduced apertures for gas separation. *J. Am. Chem. Soc.* **2020**, *142*, 4472−4480.
(39) Kratochvil, A. M.; Koros, W. J. Decarboxylation-induced crosslinking of a polyimide for enhanced CO_2 plasticization resistance. *Macromolecules* **2008**, *41*, 7920−7927.
(40) Cai, L. L.; Sun, Q.; Bao, M.; Ma, H. H.; Yuan, C. X.; Xu, W. Competition between hydrogen bonds and coordination bonds steered by the surface molecular coverage. *ACS. Nano.* **2017**, *11*, 3727−3732.
(41) Zhu, S. W.; Wang, Z. G.; Shi, Y. S.; Lai, W. K.; Zhang, Y. T.; Jin, J. Y.; Jin, J. Benzyl-induced crosslinking of polymer membranes for highly selective CO_2/CH_4 separation with enhanced stability. *Macromolecules* **2022**, *55*, 6890−6900.
(42) Song, P. A.; Wang, H. High-performance polymeric materials through hydrogen-bond cross-linking. *Adv. Mater.* **2020**, *32*, 1901244.
(43) Kosuri, M. R.; Koros, W. J. Defect-free asymmetric hollow fiber membranes from Torlon®, a polyamide-imide polymer, for high-pressure CO_2 separations. *J. Membr. Sci.* **2008**, *320*, 65−72.
(44) Fritsch, D.; Peinemann, K.-V. Novel highly permselectivity 6F-poly(amide-imide)s as membrane host for nano-sized catalysts. *J. Membr. Sci.* **1995**, *99*, 29−38.
(45) Fan, H. W.; Mundstock, A.; Feldhoff, A.; Knebel, A.; Gu, J. H.; Meng, H.; Caro, J. Covalent organic framework−covalent organic framework bilayer membranes for highly selective gas separation. *J. Am. Chem. Soc.* **2018**, *140*, 10094−10098.
(46) Jiang, Q.; Zhang, Q.; Wu, X. Y.; Wu, L. W.; Lin, J. H. Exploring the interfacial phase and $\pi-\pi$ stacking in aligned carbon nanotube/polyimide nanocomposites. *Nanomaterials* **2020**, *10*, 1158.
(47) Park, J. Y.; Paul, D. R. Correlation and prediction of gas permeability in glassy polymer membrane materials via a modified free volume based group contribution method. *J. Membr. Sci.* **1997**, *125*, 23−29.
(48) Bondi, A. A. Van der waals volumes and raddi. *J. Phys. Chem.* **1964**, *68*, 441−451.
(49) Zhang, W.; Wu, B. H.; Sun, S. T.; Wu, P. Y. Skin-like mechanoresponsive self-healing ionic elastomer from supramolecular zwitterionic network. *Nat. Commun.* **2021**, *12*, 4082.
(50) Zhao, X. H.; Chen, X. Y.; Yuk, H.; Lin, S. T.; Liu, X. Y.; Parada, G. Soft materials by design: unconventional polymer networks give extreme properties. *Chem. Rev.* **2021**, *121*, 4309−4372.
(51) Huang, M. H.; Wang, Z. G.; Lu, K.; Fang, W. X.; Bi, X. Y.; Zhang, Y. T.; Jin, J. In-situ generation of polymer molecular sieves in polymer membranes for highly selective gas separation. *J. Membr. Sci.* **2021**, *630*, No. 119302.
(52) Li, F. S.; Yang, H.; Zhuo, Q. M.; Zhou, D. H.; Wu, X. J.; Zhang, P. L.; Yao, Z. Y.; Sun, L. C. A Cobalt@Cucurbit[5]uril complex as a highly efficient supramolecular catalyst for electrochemical and photoelectrochemical water splitting. *Angew. Chem., Int. Ed.* **2021**, *133*, 2004−2013.
(53) Shishatskiy, B. S.; Nistor, C.; Popa, M.; Nunes, P. S.; Peinemann, K. V. Polyimide asymmetric membranes for hydrogen separation: Influence of formation conditions on gas transport properties. *Adv. Eng. Mater.* **2006**, *8* (5), 390.

https://doi.org/10.1021/acs.macromol.2c02594
Macromolecules 2023, 56, 3430−3439

(54) Robeson, L. M. The upper bound revisited. *J. Membr. Sci.* **2008**, *320*, 390−400.
(55) Sajjan, P.; Nayak, V.; Padaki, M.; Zadorozhnyy, V. Y.; Klyamkin, S. N.; Konik, P. A. Fabrication of cellulose acetate film through blending technique with palladium acetate for hydrogen gas separation. *Energy. Fuels.* **2020**, *34*, 11699−11707.
(56) Ahn, J.; Chung, W. J.; Pinnau, I.; Guiver, M. D. Polysulfone/silica nanoparticle mixed-matrix membranes for gas separation. *J. Membr. Sci.* **2008**, *314*, 123−133.

https://doi.org/10.1021/acs.macromol.2c02594
Macromolecules 2023, 56, 3430−3439